Discover Applied Sciences

Research

Synthesis of nitrogen-purged biochar and modification with hydrothermal activation: comparative assessment as adsorbents for effective elimination of Pb(II) and Cd(II) from wastewater

Madhumonti Saha[1,2] · Pabitra Kumar Biswas[1] · Jayanta Kumar Saha[2] · Abhijit Sarkar[2] · Sandip Mandal[3] · Dinesh Kumar Yadav[2] · Sangeeta Lenka[2] · M. Vassanda Coumar[2] · Biraj Bandhu Basak[4]

Received: 17 August 2024 / Accepted: 7 February 2025
Published online: 15 February 2025

Abstract

For sustainable development, wastewater treatment and recycling are inevitable; using adsorbents to treat wastewater is widely accepted. This article is aimed to synthesize adsorbents (novel biochars) from agricultural wastes and to investigate the adsorption behaviours of Pb(II) and Cd(II) on novel biochars. Nitrogen purged biochar (NPBC) was synthesized by pyrolysis with nitrogen purgation of wheat straw; whereas, steam activated biochar (SABC) was synthesized by pyrolysis-cum-hydrothermal (steam) activation. Synthesized NPBC and SABC were characterized by physical, chemical, XRD, FTIR, and SEM–EDX methods. SABC was more porous and amorphous in nature with higher specific surface area (SSA), but consisted relatively less polar surface functional groups than that of NPBC. The external layer of both NPBC and SABC were negatively charged ($pH > pH_{PZC}$). Results revealed that SABC exhibited 97% and 80% recovery efficiency of Pb(II) and Cd(II), respectively, while NPBC demonstrated Pb(II) and Cd(II) removal efficiencies of 87.6% and 69.4%, respectively, at initial concentrations of 50 and 5 mg L^{-1}. Adsorption of Pb(II) and Cd(II) upon SABC and NPBC occurred spontaneously, also exothermically, but decreased with increased reaction temperature. The maximum adsorption capacities (q_{max}) of NPBC and SABC for Pb(II) were 452.13 and 1117 mg g^{-1}, whereas for Cd(II) those were 314.9 and 470.43 mg g^{-1}, respectively, according to the Langmuir isotherm approach ($R^2 > 0.989$). So, SABC performed better than NPBC for removing both metals from wastewater. Both NPBC and SABC exhibit substantial prospects for regeneration and consequent adsorbent recovery. Hence, the designed adsorbents can be very effective towards cationic toxic heavy metal removal from wastewater.

Article Highlights

- Wheat straw was modified to N_2-purged biochar (NPBC) and activation with hydrothermal action (SABC) for the removal of Pb(II) and Cd(II)

Supplementary Information The online version contains supplementary material available at https://doi.org/10.1007/s42452-025-06589-y.

✉ Madhumonti Saha, madhumonti2609@gmail.com; ✉ Abhijit Sarkar, asiari2012@gmail.com | [1]Department of Soil Science and Agricultural Chemistry, Institute of Agriculture, Visva Bharati University, Sriniketan 731236, India. [2]Division of Environmental Soil Science, ICAR-Indian Institute of Soil Science, Bhopal 462038, India. [3]Division of Agricultural Energy and Power, ICAR-Central Institute of Agricultural Engineering, Bhopal 462038, India. [4]Division of Soil Science and Agricultural Chemistry, ICAR-Indian Agricultural Research Institute, New Delhi 110012, India.

- SABC proved better adsorption capacity compared to NPBC, involving physical adhesion, electrostatic attraction and transfer of ions
- Up to three recycling periods, the adsorbents indicate a satisfactory metal removal capacity offering a sustainable eccentric material

Keywords Wheat straw · Steam activated biochar · Nitrogen-purged biochar · Heavy metals · Adsorption mechanisms · Wastewater · Kinetics · Thermodynamics · Isotherm

1 Introduction

With the advancement of urbanization, civilization, and industrialization worldwide, approximately 380 billion cubic meters of wastewater are produced every year [1]. The majority of wastewater is produced by households (50–80%), with the industrial sectors contributing 20–30%, and discharged into the natural ecosystems [2]. Additionally, nearly 5500 billion cubic meters of fresh water are getting contaminated every year [2]. By 2025, it's predicted that approximately 67% of the globe's inhabitants could experience water scarcity; also, worldwide ecosystems will severely suffer due to contamination of the food chain via unsafe water [3]. Pb(II) (lead) and Cd(II) (cadmium) are a pair of heavy metals (HM) that are discharged into the environment through mining, manufacturing, and agricultural activities, domestic effluent discharge, and natural mineral weathering and volcanic phenomena [4]. A concentration of Pb or Cd above 0.05 mg L^{-1} in drinking water can cause multiple diseases in humans, sometimes resulting in fatality [5]. For example, prolonged exposure to Pb may result in reproductive disorders, cardiovascular problems, kidney damage, impaired brain development and renal function, elevated blood pressure, and increased risk of hypertension in humans [6]. Similarly, exposure to Cd, even at a low level, may alter bone composition (Itai-itai disease) and renal failure in humans [6]. A concentration of Pb or Cd above 5 mg L^{-1} in irrigation water often causes severe toxicity in plants, impacting crop growth and yield and increasing the possibility of transfer of these metals into the human body through food [5]. Therefore, it is crucial to treat wastewater and lower the levels of heavy metals, including Pb and Cd, before using it for alternative purposes.

Various physico-chemical and biological techniques, including flocculation, membrane-based filtration, electrolysis, adsorption, ion exchange, and complexation, can be employed to eradicate heavy metal ions from wastewater [7–10]. Most of the above-mentioned methods have several limitations such as expensive, secondary pollutant creators, toxicity enhancer and requirement of longer period. Over other techniques, the adsorption process has a number of advantages, such as low-cost involvement, low energy consumption, reusability for use, operational design flexibility, and robust working conditions [11, 12]. The issue with financial commitment in the source accessibility could be resolved by using waste materials of biological origin, such as agricultural residues, as adsorbents [13]. Wheat straw, which biochemically is composed of lignin, cellulose, and hemicellulose, is a well-known biosorbent of HM ions [13]. Wheat straw adsorbents contain ether, carbonyl, and hydroxyl functional groups, which are essential for binding HM ions through chelating, complexing, coordinating, electrostatic attraction, and hydrogen bonding mechanisms [14, 15]. However, pristine wheat straw adsorbents suffer from low HM removal capacity due to restricted surface area, fewer active sites for adsorption, and fewer hydroxyl, carbonyl, and methoxy groups present on the surface [16, 17].

Improving the HM adsorption ability of agricultural residue-based adsorbent is of continuing interest to researchers, and this has often been attempted to achieve through chemical and/or physical modification of the raw materials [11, 18]. Among the modification methods, conversion of crop residues into biochar (BC) through pyrolysis and use of the biochar for removing HM from wastewater have received tremendous momentum in the last decade [19]. For example, BC from wheat straw had a comparatively higher particle surface area as well as porosity with a multi-channel micropore structure in comparison to pristine wheat straw [20, 21]. Fe-functionalized wheat straw biochar had a higher Cd(II) adsorption capacity (82.84 ppm); additionally, greater removal efficiency for Pb(II), which was (111.24 ppm) from wastewater, and better regeneration ability [14]. Wheat straw is a by-product that is acquired following the wheat harvest which is the second abundant agricultural waste biomass; about 354 million tons of wheat straw are generated worldwide [22]. 37–40% cellulose, 21–25% hemicelluloses, and 11–22% lignin was found in the compositional analysis of wheat straw [13]. The traditional wheat straw management practice in India is in-field burning, which is detrimental to the environmental quality and human well-being [23, 24]. Converting wheat straw to biochar and using the biochar for HM removal from water thus offers an opportunity to tackle multiple environmental issues, including air pollution, water and soil contamination, and agricultural waste recycling.

Biochar is becoming increasingly popular as a potential low-cost alternative to costly activated carbons [25, 26]. Biochar often exhibits improved adsorption qualities over the unprocessed original biomass of agro-waste through significant physical and chemical changes that typically include an increase in surface area, pore volume and changes in surface chemistry (more functional groups) that make biochar more effective at adsorbing various substances. Poplar biochar had a higher Cr(II) and Cu(II) adsorption capacity (27.9 and 31.7 μmol g^{-1}) compared to original feedstock (14.9 and 9.1 μmol g^{-1}); similarly, corn biomass is less effective in removing Cr(II) and Cu(II) (35.7 and 13.4 μmol g^{-1}) in comparison with corn biochar (109 and 128 μmol g^{-1}) from wastewater, and lower regeneration ability [27]. Furthermore, pomegranate peel derived biochar 290.04 mg g^{-1}) better performs as adsorbent compared to original feedstock (77.87 mg g^{-1}) for dye removal from wastewater [28]. Moreover, increasing the specific surface area of biochar improved the adsorbent's ability to remove HM [29]. Activation of biochar with steam in a hydrothermal treatment was reported to increase the specific surface area of biochar significantly [30]. Additionally, the steam activation could increase the proportion of responsive functional groups of biochar's surfaces that facilitate HM adsorption via promoting various binding mechanisms [31]. To date, several studies have concentrated on the heavy metal elimination from wastewater using pristine as well as modified biochar; however, a few studies have focused on wheat straw biochar produced via N_2 purging. However, short of information is available regarding lead and cadmium removal using steam activated wheat straw biochar (SABC). There is a need for more research on developing cost-effective and environmentally friendly simple technologies to scale up biochar-based heavy metal removal. The originality of our effort comprises utilization of residual wheat straw, which would otherwise be burned in field causes environmental pollution. This raises the viability of pyrolysis economically and provides a sustainable water treatment solution that aligns with the circular economy's tenets. Additionally, the energy intensive carbonization and activation techniques are utilized in preparing biochar, therefore, biochar are regenerated or recycled for several adsorption cycles in this study, which improved its economic viability. A comparative assessment of SABC with N_2 purged biochar (NPBC) in terms of their physico-chemical properties contributing to interactive mechanisms for HM removal is also a least reported area. Here we hypothesize that the steam activation of wheat straw biochar will improve the SSA via enlargement of internal cavities and increased microporosity that would then result in higher HM removal by the activated biochar through physisorption. The objectives of this study are (1) to synthesize NPBC from wheat straw and modify it via hydrothermal activation to obtain SABC; (2) to thorough characterization of the NPBC and SABC using state-of-the-art analytical methods; and (3) to study the adsorption kinetics, isotherm and thermodynamic properties of Pb(II) and Cd(II) on NPBC and SABC, as well the key mechanisms of adsorption. Simply, SABC demonstrated superior repurposing potential with three times reusability as adsorbent materials.

2 Materials and methods

2.1 Reagents and materials

Wheat straw (WS) (*Triticum aestivum* L.) feedstock was collected from the research farm of the Indian Council of Agricultural Research-Indian Institute of Soil Science, Bhopal (23.3078° N, 77.4069° E) to prepare the biochar. As analyzed on a CHN analyzer (Thermofisher SCIENTIFIC NC Flash 2000, USA), the C and N contents of the wheat straw were 40.1 and 0.3%, respectively and the average moisture content is 11–12%. Analytical-grade lead nitrate ($Pb(NO_3)_2$) and cadmium nitrate tetrahydrate ($Cd(NO_3)_2$. $4H_2O$) had been procured via Merck India Limited. Other reagents were obtained from HiMedia Laboratories Pvt. Ltd.

2.2 Synthesis of N_2-purged and steam-activated biochar

The procedure of the biochar preparation in this study was done by the following method. The first step in this procedure is to wash the wheat straw with deionized water. Following washing, the wheat straw was further exposed to natural drying and grinding with a dry biomass grinder to a size of less than 2.5 mm. Then it was powdered to a size of < 1 mm. The goal of the drying process is to remove any remaining moisture before the pyrolysis process, which produces biochar. Biochar was prepared through pyrolysis of that dried and processed wheat straw in a custom-designed batch type tubular stainless-steel pyrolysis reactor (length 600 mm and internal diameter 100 mm). The pyrolysis reactor was fabricated and optimized for operation at the Indian Council of Agricultural Research-Central Institute of Agricultural Engineering, Bhopal [32, 33]. A K-type thermocouple was installed in the reactor's centre that measured the temperature inside the reactor. Each batch of pyrolysis accommodated 0.2 kg of dried and processed

wheat straw feedstock. Before loading of the feedstock, N_2 gas purging into the reactor was adjusted to a constant rate of flow rate of 3 L min^{-1}. The NPBC was obtained via wheat straw pyrolysis with N_2 purging conditions for 2 h at 700 °C. The SABC was obtained by combining the above N_2 purging with a steam activation during the pyrolysis process. Steam was generated by a steam generator using distilled water at 2 bar pressure and was connected to the reactor to supply steam at a rate of flow of 5 L min^{-1} throughout the pyrolysis for 2 h. The reactor was turned off after 2 h (the steady state persisted) of operation, then synthesized SABC and NPBC were transferred from the reactor when the temperature attained 30 °C, then traversed via a 0.149 mm sieve to separate the fine fractions of biochar. The C% and N% of the NPBC were 48.7 and 28.3%, respectively; whereas those were 69.5 and 0.58%, respectively, in the SABC (Table 1).

2.3 Characterizations of NPBC and SABC

Fourier transformed infrared (FTIR) spectroscopy (Thermo Scientific™ Nicolet™ iS5™ FTIR spectrometer, USA; installed with fast recovery DTGS detector) was used to examine (with KBr palette) the formation of new bonds and the breaking of previous ones within the WS, NPBC, and SABC structures prior to and following Pb(II) and Cd(II) adsorption. Each sample was scanned with a 0.5 cm^{-1} scanning resolution between 400 and 4000 cm^{-1} in the infrared spectrum. To evaluate the crystallinity and amorphous nature of WS, NPBC, and SABC, an X-ray diffractometer equipped with Automated Powder Diffraction software (Philips™ PW1710™, Slovak Republic) was used to record the XRD patterns of the powdered adsorbents. Continuous scanning of the X-ray was performed from a 4 to 50° angle of 2θ at a speed of 2θ s^{-1} (0.025) under Ni-filtered monochromatic Cu-Kα, where λ = 0.15418 nm. The benchtop type SEM–EDX (SEM model: JEOL JSM 5600, Tokyo, Japan) was employed to describe the surface configuration and chemical analysis of the NPBC and SABC, with a tungsten filament as the electron source. This allowed for the analytical elemental analysis to be performed using the attached energy dispersive X-ray (EDX) system. The Ethylene Glycol Mono-ethyl Ether method was used to calculate the total surface area of NPBC and SABC, and a standard procedure described by Carter et al. [34] was used to calculate the specific surface area (m^2 g^{-1}), which is defined as the total surface area per unit mass. To investigate the surface properties of the adsorbents, the point of zero charge (pH_{PZC}) was ascertained in triplicates utilizing the technique of solid addition [35]. Diluted HCl and NaOH were used to adjust the initial pH (pH_i) of each flask comprising 0.01 M and 0.1 M KNO_3 (50 mL of each solution) to a value between 1 ± 0.2 and 13 ± 0.2. Adsorbent (50 mg) was added to each solution, and the mixtures were stirred for an entire day at room temperature. The pH_{PZC} value is obtained by plotting ΔpH (pH_f—pH_i) opposed to pH_i after the final pH (pH_f) of the solutions has been measured.

Table 1 Physicochemical properties of biochars

Parameters	NPBC	SABC	Methods
pH (1:5)	10.94 ± 0.21	10.86 ± 0.15	pH and EC meter
EC (1:5)(dS m^{-1})	4.99 ± 0.14	4.31 ± 0.26	
Total C (%)	48.70 ± 2.15	69.50 ± 1.05	EDS Spectra analysis
Total N (%)	27.33 ± 1.74	0.58 ± 0.04	
Total O (%)	14.79 ± 0.96	20.85 ± 0.53	
Total Si (%)	1.69 ± 0.10	2.69 ± 0.21	
Total P (%)	0.59 ± 0.04	ND	
Total- K (%)	4.02 ± 0.10	4.29 ± 0.27	
Total Ca (%)	0.63 ± 0.02	0.65 ± 0.03	
Total Mg (%)	0.07 ± 0.01	0.07 ± 0.00	
Total Fe (%)	0.30 ± 0.02	0.13 ± 0.02	ICP-OES analysis
Total Mn (μg g^{-1})	131.50 ± 4.85	119.93 ± 4.72	
Total Cu (μg g^{-1})	30.66 ± 1.55	42.93 ± 4.31	
Total Zn (μg g^{-1})	48.00 ± 2.26	36.06 ± 2.72	
Specific surface area (m^2 g^{-1})	270.00 ± 4.70	326.00 ± 6.30	EGME

NPBC Nitrogen purged biochar, *SABC* Steam activated biochar

2.4 Batch adsorption experiments

The effects of different factors: shaking time, temperature, pH, concentration of metal ions, and dosage of the adsorbent regarding Pb(II) and Cd(II) adsorption were investigated using batch adsorption experiments with synthetic wastewater. To create synthetic wastewater with Pb and Cd, 1.6 g of $Pb(NO_3)_2$ and 2.74 g of $Cd(NO_3)_2$. $4H_2O$ were dissolved, respectively in one liter of distilled water. Then, diluted the solution to the desired concentration. The elimination of Pb(II) and Cd(II) by NPBC and SABC were studied as functions of one factor by varying its range while keeping all other factors constant with respect to their optimum conditions. Each of the batch of experiments was conducted with BCs in Pb(II) and Cd(II) solutions of 50 mL in a centrifugal tube. To reach equilibrium, biochar mixing with Pb(II) and Cd(II) solutions separately was shaken and centrifuged for 5 min at 2000 rpm, then filtered through Whatman No. 42 filter paper. The concentrations of Pb(II) and Cd(II) were measured by ICP-OES (Model: Perkin Elmer® Avio® 560 Max ICP-Optical Emission Spectrometer, Shelton, USA) both in solution and adsorbed phase. Optimum operating conditions for metal determinations by ICP-OES were maintained with power 1.2 kW, plasma gas flow rate 15 L min^{-1}, nebulizer gas flow rate 0.80 L min^{-1}, sample flow rate 0.80 L min^{-1} and the wavelengths for Pb and Cd were 220.35 and 214.44 nm, respectively. No adsorbent was used in blank tests to ensure that HM precipitation has no effect on metal adsorption.

Every batch adsorption experiment was carried out in three replicates, and the mean of the quantitative results was taken into account for subsequent calculations. Additionally, the data's comparative standard deviation was calculated.

2.4.1 Adsorption kinetics

Effective shaking time for the elimination of Pb(II) as well as Cd(II) from by the adsorbents were found by varying their shaking time from 0 to 360 min by keeping other experimental conditions constant (where, initial concentration metal ions 50 mg L^{-1} for Pb(II) and 5 mg L^{-1} for Cd(II), solution pH 5.0 ± 0.2, dosage of adsorbent 10 g L^{-1}, and temperature 298 K).

2.4.2 Adsorption isotherm

Pb(II) and Cd(II) elimination by adsorbents (NPBC and SABC) were determined by varying initial concentrations of Pb(II) (0 to 200 mg L^{-1}) and Cd(II) (0 to 10 mg L^{-1}) with constant solution pH 5.0 ± 0.2, dosage of adsorbent 10 g L^{-1}, shaking time 60 min, and temperature 298 K.

2.4.3 Adsorption thermodynamics

To assess the adsorption thermodynamics, adsorption experiments were conducted in different batches at 298, 308, and 318 K by keeping other experimental conditions constant (initial metal concentration of Pb(II) (50 mg L^{-1}) and Cd(II) (5 mg L^{-1}), solution pH 5.0 ± 0.2, dosage of adsorbent 10 g L^{-1}, and shaking time 60 min).

2.4.4 Solution pH and adsorbent doses

Solution pH was modified from 3.0 ± 0.2 to 8.0 ± 0.2 with 0.1 N HCl and 0.1 N NaOH and kept other factor constants (Pb(II) conc. 50 mg L^{-1} and Cd(II) conc. 5 mg L^{-1}, dosage of adsorbent 10 g L^{-1}, shaking time 60 min, and 298 K temperature). Effective dosage of NPBC and SABC for the elimination of Pb(II) and Cd(II) from fabricated wastewater was optimized by changing adsorbent dosages from 0 to 40 g L^{-1}.

2.4.5 Desorption and reusability performances

To explore the reusability of the NPBC and SABC desorption experiments were conducted. The Pb(II) and Cd(II) loaded NPBC and SABC samples (dried for 24 h at 60 °C after adsorption experiment) were shaken with 0.2 *N* HCl (50 mL) at 180 rpm for 30 min and then centrifuged for 10 min at 3000 rpm. After extracting the supernatant, adsorbents were rinsed with deionized water to remove the excess acid. Using the same adsorbents, the adsorption–desorption cycle was repeated three times. The baseline concentrations of Pb(II) and Cd(II) were 200 mg L^{-1} and 10 mg L^{-1}, respectively, in each cycle. Desorbed

Pb(II) and Cd(II) concentrations within the removed supernatant were analyzed by ICP-OES. The adsorption efficiency of the above HM ions onto NPBC and SABC for each cycle was calculated. Each test was conducted with three replications, and the mean was computed.

2.5 Data analysis and modelling

Q_t (mg g^{-1}), the adsorption capacity, and R (%), the removal efficiency of Pb(II) and Cd(II) by NPBC and SABC at equilibrium was calculated using Eq. 1 and Eq. 2 following [36].

$$q_t = \frac{(C_0 - C_e)\,V}{m} \tag{1}$$

$$R(\%) = \frac{(C_0 - C_e)}{C_0} \times 100 \tag{2}$$

The variables C_0 and C_e represent the initial and equilibrium adsorbate concentration (mg L^{-1}), V denotes the total volume of adsorbate (L), and m signifies the amount of adsorbent (g).

2.5.1 Adsorption kinetic models

Non-linear pseudo-first order (PFO) (Eq. 3), pseudo-second order (PSO) (Eq. 4), Elovich (Eq. 5) and intra-particle diffusion model (Eq. 6) were applied to determine the best fit for Pb(II) and Cd(II) [37].

$$q_t = q_e\left(1 - e^{k_1 t}\right) \tag{3}$$

$$q_t = \frac{q_e^2 k_2 t}{(1 + q_t k_2 t)} \tag{4}$$

$$q_t = \frac{1}{\beta} ln(\alpha\beta t + 1) \tag{5}$$

$$q_t = k_{diff} t^{1/2} + C \tag{6}$$

where k_1 is the PFO rate constant (min^{-1}), t is the time (minute), k_2 is the PSO rate constant (g mg^{-1} min^{-1}), k_{diff} is the intra-particle rate constant (mg g^{-1} $min^{-1/2}$), C is the plot's intercept, α is the original rate of adsorption (mg g^{-1} min^{-1}), and β is the degree of surface coverage (g mg^{-1}). The quantity of metal adsorbed (mg g^{-1}) at time t and at equilibrium is denoted by q_t and q_e.

2.5.2 Adsorption isotherm models

Non-linear isotherm models viz. Langmuir (Eq. 7), Freundlich (Eq. 8), Redlich-Peterson (Eq. 9) and Temkin (Eq. 10) equation comprehend the interaction of Pb(II) and Cd(II) with NPBC and SABC surface and the values were computed using following equations [38].

$$q_e = \frac{K_l C_e q_m}{(1 + K_l C_e)} \tag{7}$$

$$q_e = K_f C_e^{1/n} \tag{8}$$

$$q_e = \frac{(K_{rp}C_e)}{(1 + \alpha C_e^{\beta})} \tag{9}$$

$$q_e = \frac{RT}{b_T} In(K_T C_e) \tag{10}$$

where, the equilibrium adsorbate (mg g^{-1}) loaded over the adsorbent is denoted by q_e. Ce is the heavy metal released at equilibrium (mg L^{-1})., q_m is Langmuir HM maximum adsorption potentiality (mg g^{-1}), K_l is the Langmuir constant (L mg^{-1}) pertaining to the energy of metal binding, K_f is the Freundlich constant (mg $^{-1}$), n is the Freundlich exponent (L g^{-1}) associated to the energy of metal binding, K_{rp} is the Redlich–Peterson isotherm constant (L g^{-1}), α is the another constant (L $mg^{-1})^{\beta}$ and β is the exponent shows the adsorbent's heterogeneity, which varied from 0 to 1. R is the universal gas constant (J mol^{-1} K^{-1}), $T$is the temperature (Kelvin), K_T is the equilibrium constant for binding (L g^{-1}), b_T is the constant associated to sorption heat (J mol^{-1}).

2.5.3 Adsorption thermodynamics

Van't Hoff's equations were used to compute and assess the thermodynamic variables, such as changes in Gibb's free energy (ΔG) [39]:

$$\Delta G = \Delta H - T\Delta S \tag{11}$$

$$\Delta G = -RT\,\ln K \tag{12}$$

$$\ln K = (\Delta S/R) - (\Delta H/RT) \tag{13}$$

Here, T is the temperature (K), K represents the dispersion coefficient of the metal ions that exist between the adsorbed stage and the rest of the aqueous solution ($K = C_A/C_e$), where $C_A = (C_0 - C_e)$ represents the adsorbed amount of adsorbate (mg L^{-1}) at equilibrium and Ce denotes equilibrium concentration (mg L^{-1}) in solution. ΔG is the change in Gibb's free energy (KJ mol^{-1}); ΔH symbolizes the enthalpy changes (KJ mol-1); and ΔS indicates the entropy changes (J mol^{-1} K^{-1}).

R-square (R^2) were used to express the goodness of fit of the regression model, and analysis of variance (ANOVA) was used to assess both the kinetics and isotherm models. R^2 and Chi-square (χ^2) were used to assess the suitability of these models after the non-linear methods of the kinetic and isotherm models and they were fitted to the experimental data using OrigingPro9 software®.

3 Result and discussion

3.1 Characterization of NPBC and SABC

3.1.1 XRD, SEM–EDX and specific surface area analysis

The XRD patterns of NPBC and SABC are presented in Fig. 1a. WS has a semi-crystalline structure: two medium-shaped humps (15° and 24° 2θ), and one sharp peak at 27.6° (2θ), respectively (Fig. S1, supplementary information). These signals are the outcome of inter- and intra-molecular H-bonding between the functional groups observed in the cellulolytic units, as well as their orderly arrangement by the cellulolytic backbone [40]. The two diffraction peaks of WS gradually lose intensity and merge into a single wide peak between 10° and 20° (2θ) due to the tiny crystallite dimensions that are vertical to the aromatic layers [16, 17]. Nevertheless, two small peaks were observed for NPBC at 23° and 28.2° (2θ) with increased pyrolysis Tat 700 °C. Sharp and unlabelled peaks in NPBC represent several inorganic components [41]. The development of a polyaromatic graphite-like structure was validated by the NPBC XRD peaks. However, no distinctive peak was observed for SABC within the range of 20° to 50° (2θ). The disordered nature of the straw biochar indicated the broadened peak in XRD in another literature [42]. This indicates the disordered nature of the activated carbon. Turbostatic carbon crystallites are developed due to the enlargement of the peak in the XRD pattern of the SABC material, which was caused by the destruction of the crystalline character of the original WS [41].

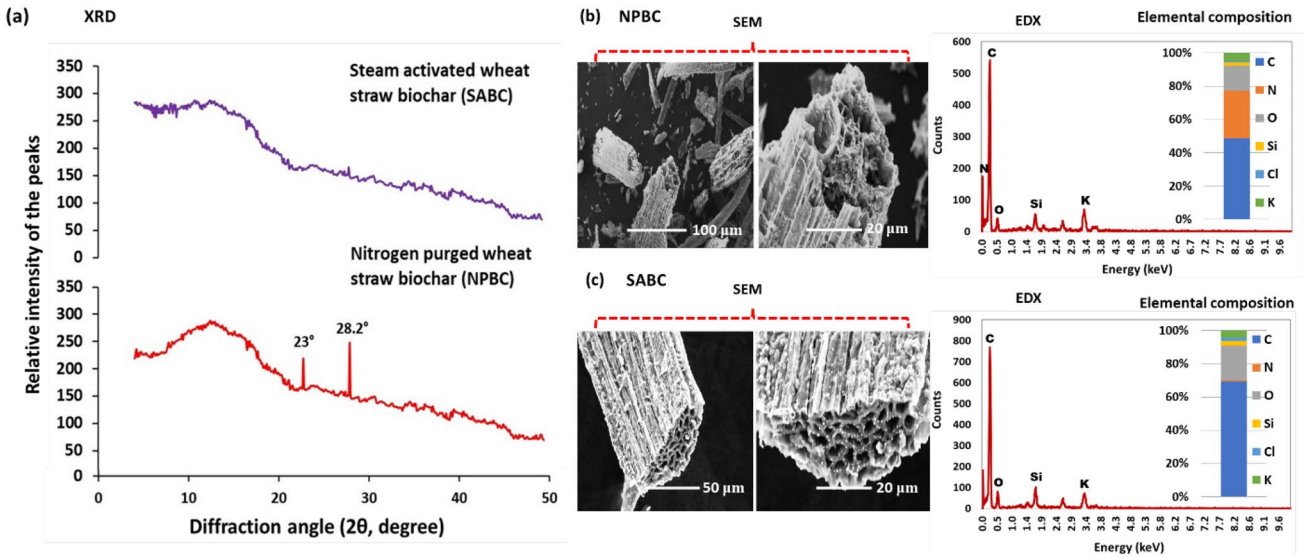

Fig. 1 XRD-patterns (**a**) and SEM–EDX images of Nitrogen-purged biochar (NPBC) (**b**) and steam activated biochar (SABC) (**c**)

Figure 1b, c depicted surface morphology (SEM images) of NPBC and SABC at different magnifications. SEM images of NPBC showed the presence of several hollow cylindrical pores derived from plant cells with a polyaromatic graphite-like framework and large surface area [42]. The predominancy of C (48.7%), N (28.3%), and O (14.8%) in EDX spectra of NPBC confirmed that the most skeleton component was C-linked with N- and O-containing functional groups, viz., -C = O and -CONH, along with the presence of additional components such as Si and K. SEM images of SABC showed the presence of several hollow cylindrical pores derived from plant cells with honeycomb structures and high surface area. The EDX spectra of SABC in Fig. 1b, c indicated the dominancy of C (69.5%) and O (20.8%) which confirms that the maximum skeleton component was C, which was associated with O-comprising functional groups like C = O and COOH along with the presence of other elements, *i.e.,* Si and K.

The EGME method was done to analyze the adsorbent's specific surface area before HMs adsorption, and their values are presented in Table S1 (Supplementary information). It was previously stated that EGME has an advantage over the gas adsorption method as it is able to explore the internal surface area of clay minerals (interlayer surfaces) and organic substances (i.e., internal pore spaces induced by multipolymeric arrangements with cellulolytic structure), which are relevant under natural environmental conditions but inaccessible under dry situations during the process of gas adsorption [43]. The SSA of WS, NPBC, and SABC was found to be 218.1, 270.6, and 326.4 $m^2\ g^{-1}$, respectively. The SSA of NPBC was 24% and SABC was 49.6% higher than normal WS. Previous articles reported that biochar must have a large surface area with high effective pore size in order to adsorb the pollutants [25, 44–46].

3.1.2 FTIR and point of zero charge

Numerous functional groups on the outer layer of NPBC and SABC, both prior to and following the removal of Pb(II) and Cd(II) and their feedstock (WS), are shown in Fig. 2. The stretching of -OH groups is responsible for the absorption band at 3615 cm^{-1}, according to the FTIR spectrum of the WS. The glucose unit's bending and twisting vibrations of the C-H group are attributed to the bands at 2917 cm^{-1} and 1595 cm^{-1} [47]. The sign at 1038 cm^{-1} is attributed to the -C-O- group present in ethers and auxiliary alcohols within the cellulose chain structure [14]. Predominantly, the core functional groups of NPBC consist of signals at 1060 cm^{-1} (C–O–C, C = O), 1540 cm^{-1} (C = O, C = C, -CONH-, $-CH_2-$ and $-CH_3$), and 3770 cm^{-1} (aromatic and aliphatic O–H) [48]. Specifically, the peaks of FTIR at 3114, 1540, 1060 and 456 cm^{-1} slightly shifted to 3413, 1560, 1078 and 479 cm^{-1} when Pb(II) was adsorbed on NPBC. When Cd(II) was adsorbed onto NPBC, the change of some peaks was significantly observed. The peaks of FTIR at 1540, 1060 and 456 cm^{-1} shifted to 1558, 1032 and 479 cm^{-1} after Cd(II) adsorption on NPBC. To be precise, the main functional groups of SABC include 982 cm^{-1} (C = O, C–O–C), 1507 cm^{-1} (C = C, C = O, $-CH_2-$, $-CH_3$ and -CONH-) and 3063 cm^{-1} (aliphatic C-H) and 3648 cm^{-1} (aromatic and aliphatic O–H) [41]. Steam activation breaks down functional groups like carboxyl and phenol, which can reduce the polarity of biochar and that was noticed in the shifting of FTIR peak from 456, 1540 and 3114 cm^{-1} to 439, 1507 and

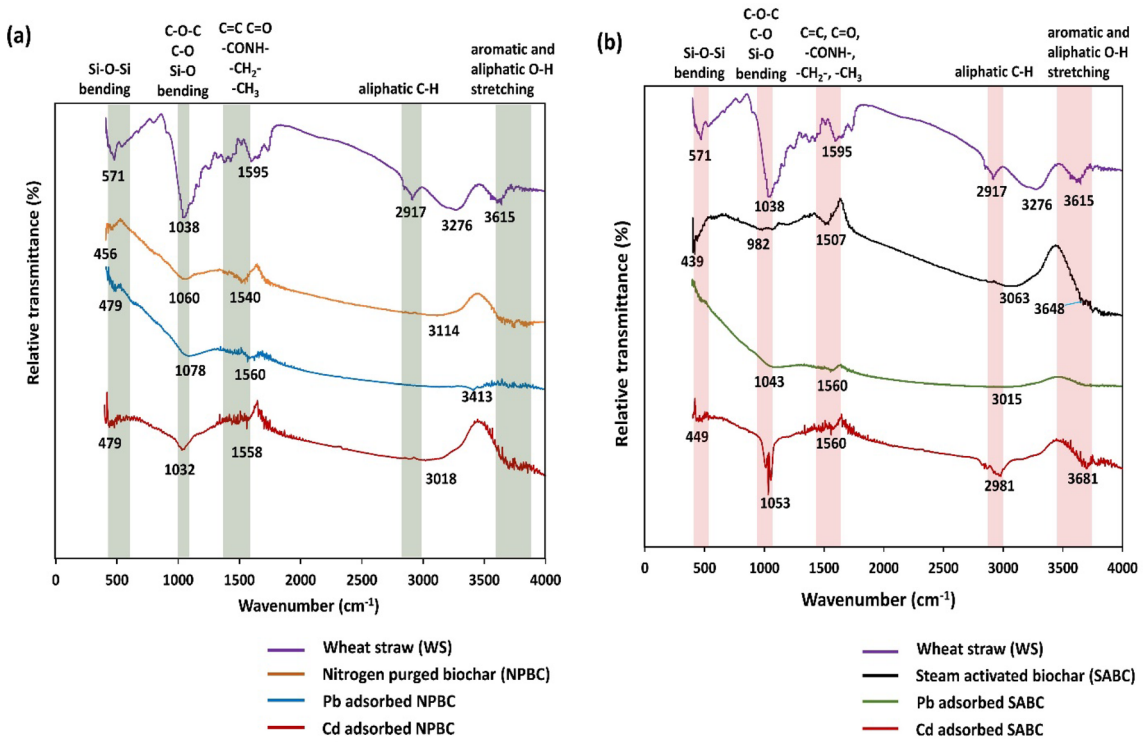

Fig. 2 FTIR spectra of (**a**) Nitrogen-purged biochar (NPBC), Pb(II) adsorbed NPBC, Cd(II) adsorbed NPBC and (**b**) Steam activated biochar (SABC), Pb(II) adsorbed SABC, Cd(II) adsorbed SABC

3063 cm^{-1}, respectively when comparing NPBC with SABC. Upon the loading of Pb(II) and Cd(II) on SABC, specifically the peaks of FTIR at 439, 982, 1507, 3063 and 3648 cm^{-1} shifted to 449, 1053, 1560, 2981, 3681 cm^{-1}, when Cd(II) was adsorbed. In Pb and Cd adsorption, the cyclic aromatic functional groups can function as π electron donors. In addition, lesser number of FTIR peak was observed when SABC was loaded with Pb(II) since there are no aliphatic or aromatic -OH containing functional groups. That indicated Pb(II) is more adsorbed by both NPBC and SABC as compared to Cd(II). So, the aromatic functional groups C = C, C = O, C–O–C, $-CH_2-$, $-CH_3$, -CONH- and aliphatic C-H obviously changed when the NPBC and SABC interacted with Pb(II) as well as Cd(II) [29].

The pH_{PZC} of NPBC sample was observed at 9.1 and 9.5 for 0.1 M and 0.01 M KNO_3, respectively (Fig. 3); whereas, the pH_{PZC} of SABC is 9.3 and 9.8 for 0.1 MKNO_3 and 0.01 M KNO_3 solutions, respectively. When $pH < pH_{PZC}$ value, the adsorbents' entire surface is assumed to be positively charged, whereas when $pH > pH_{PZC}$ value, the entire surface of the adsorbents is considered to be negatively charged [21, 45]. For both NPBC (pH 10.9) and SABC (pH 10.9)

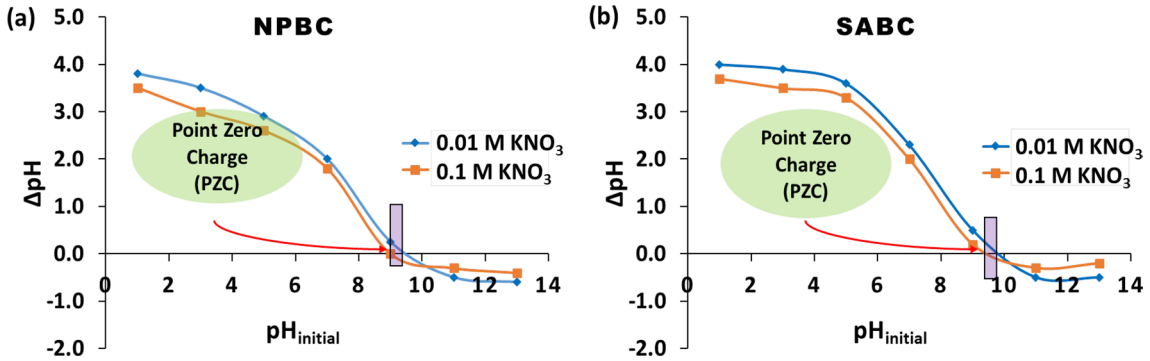

Fig. 3 ΔpH intersects pHi axis for determining Point Zero Charge (PZC) of (**a**) NPBCand (**b**) SABC.Vertical error bars denote standard deviation which represents the variation relative to corresponding mean point where n = 3

pH > pH_{PZC}, which indicated their entire surfaces are negatively charged, caused deprotonation of the active spots on the adsorbent and binding of Pb(II) and Cd(II) at the given spots in the adsorbent structure [49].

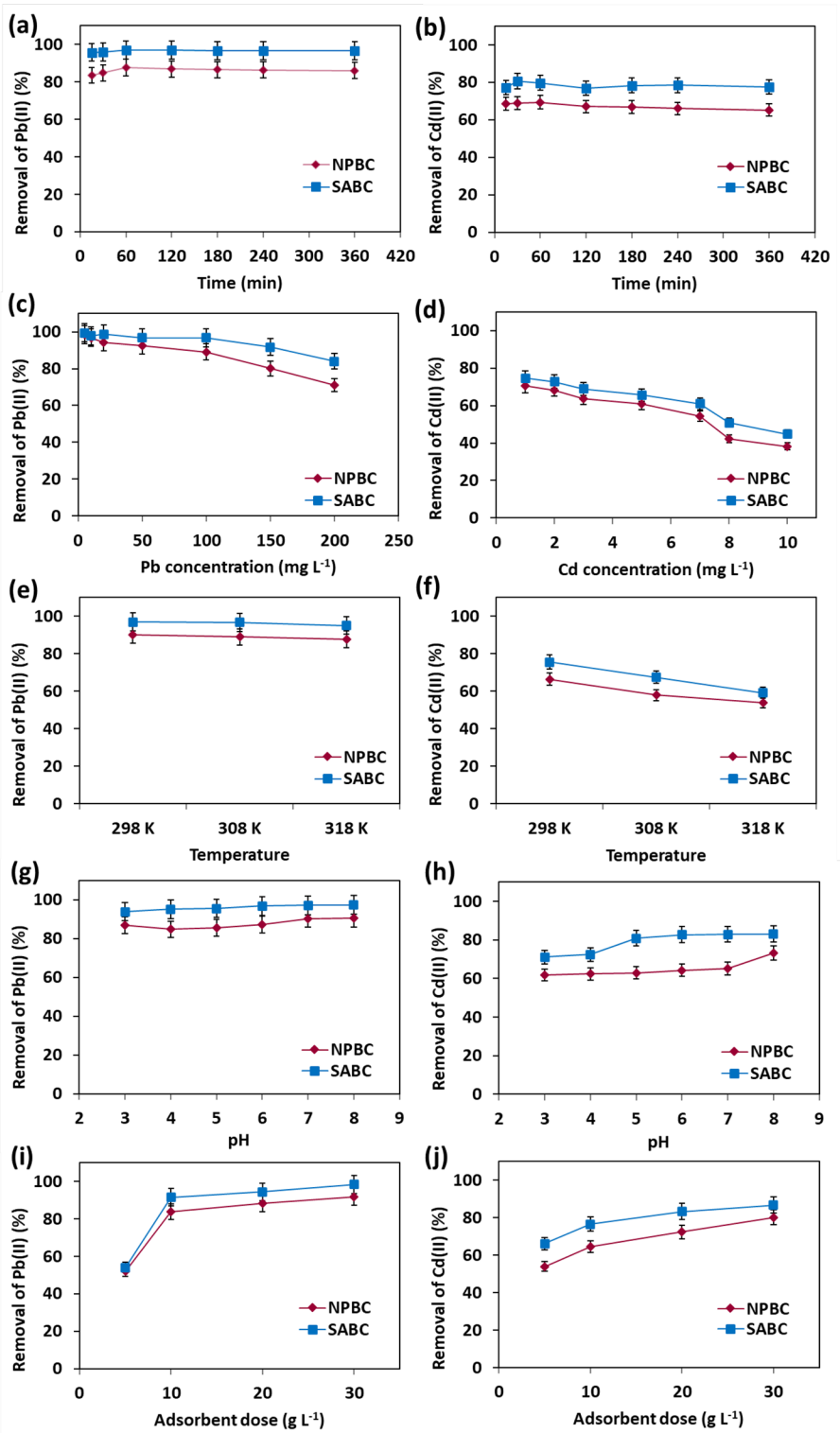

Fig. 4 Effect of contact time (**a**, **b**), metal ion concentration (**c**, **d**), temperature (**e**, **f**), pH (**g**, **h**) and adsorbent doses (**i**, **j**) on Pb(II) and Cd(II) removal efficiency of NPBC and SABC. Vertical error bars denote standard deviation which represents the variation relative to corresponding mean point where n = 3

3.2 Optimization of Pb(II) and Cd(II) removal conditions

3.2.1 Effects of contact time

Removal efficiency of Pb(II) and Cd(II) was attained steady value at 60 min (Fig. 4a, b). SABC outperforms NPBC in terms of eradication of both Cd(II) and Pb(II) from synthetic wastewater. The highest Pb(II) removal efficiency of both NPBC (87.6%) and SABC (96.9%) was found at 60 min. Similarly, the 60-min period revealed the maximum Cd(II) removal efficiency of both NPBC (69.4%) and SABC (80%) and reaches equilibrium and both the adsorbent showed higher adsorption capacity (Fig. S2a, b). Numerous vacant binding sites on the external surface of the NPBC and SABC are accountable for the rapid adsorption during the initial stage, and consequently, the solute molecules' repellent interactions between the solid and bulk phases made it difficult to occupy the remaining available sites [50]. When saturation was achieved at the outer periphery of the adsorbent, then the metal ions would enter into the pore spaces of the adsorbent and are absorbed by the interior surfaces of the adsorbent [51].

3.2.2 Effects of heavy metal ion concentration

The removal rate decreased from 98.6 to 71.2% for NPBC as the Pb(II) concentration increased from 5 to 200 mg L^{-1}, whether relatively less change from 99.4 to 84% was observed for SABC (Fig. 4c, d). At low concentrations, the majority of adsorption sites allow HM ions to attach to the adsorbent's surfaces immediately through ionic interactions [52]. With increasing metal ion concentration, adsorption capacity increased for both NPBC and SABC, however, SABC exhibited more adsorption capacity compared to NPBC (Fig. S2c, d). Adsorption would have theoretically reached a plateau after all of the binding sites of the adsorbent's surfaces were occupied because of continuous adsorption. Interestingly, there was a consistent drop in the adsorption percentage as the amount of HM ions increased [53]. Removal percent of SABC drops from 74.6% at 1 mg L^{-1} to about 44.7% at 10 mg L^{-1} indicated that Cd(II) adsorption decreases on increasing the Cd(II) concentration; similar trends were also observed for NPBC. Consequently, there is a decrease in the rate at which Cd(II) ions move from the bulk solution to the surface of the adsorbent particle.

3.2.3 Effects of temperature

Pb(II) and Cd(II) removal percent was decreased with increasing solution T from 298 to 318 K (Fig. 4e, f), which indicated that HM ion adsorption onto adsorbents is physisorption in nature. NPBC and SABC both slightly showed better adsorption percentages from 87.6 to 90% and 95 to 97%, respectively, for Pb(II) with decreasing T. Whereas, SABC showed better Cd(II) adsorption (75.5%) in comparison with the NPBC (66.4%) (Fig S2e, f). The decrease in adsorption may be due to vulnerable electrostatic bonds between the metal ions and the biochar at higher temperatures [54]. Higher temperature causes the surface layer to become thinner, allowing metal ions to migrate from the biomass surface into the solution phase and eventually desorb from the adsorbent surfaces. As a result, lowering the T is better for non-ionic exchange adsorption, indicating that the adsorbents removed the HMs by undergoing a non-ionic exchange with the HM ions.

3.2.4 Effects of solution pH

Pb(II) and Cd(II) removal percent improved with the rising solution pH from 3 to 8 (Fig. 4g, h). The pH of the HM ion solution influences both the adsorbent and metal ion by altering the surface and degree of ionization. Beyond pH 4, the removal percent of Cd(II) by NPBC and SABC were increased continuously to about 73.2% and 82.8% at pH 8. For NPBC and SABC, Pb(II) removal percent a little bit increased from 86.8 to 90.5% and 93.8 to 97.2%, respectively, within the pH range from 3 to 8. Comparatively both the adsorbents showed higher adsorption capacity at pH 8 (Fig. S2g, h). The concentration of H + declines as the pH of the solution rises. Thus, decreasing H^+ competence with Pb(II) and Cd(II) on the adsorbent surface increases adsorption capacity [55]. Specifically, at pH ≥ 8 for Cd(II) and pH ≥ 6 for Pb(II), the -OH groups will initiate to develop complexes or precipitates, generating $Cd(OH)^+/Cd(OH)_2$ and $Pb(OH)^+/Pb(OH)_2$ in the solution, respectively. This will increase the adsorption of Cd(II) and Pb(II) [56, 57]. In addition, oxygen-containing groups on the adsorbent's surface dissociate more readily at high pH values. Consequently, the

adsorbent's surface is saturated with negative charge, which promotes electrostatic attraction between them and enhances adsorption of positively charged metal ions onto their surface [58].

3.2.5 Effects of adsorbent doses

The removal efficiency of Pb(II) enhanced from 51.9 to 91.8% and 54 to 98.3% for NPBC and SABC, respectively, when the dose is augmented from 5 to 40 g L^{-1} (Fig. 4i, j). Besides, Cd(II) removal efficiency increased from 66.1 to 86.7% with increasing doses of SABC. However, maximum adsorption of Cd(II) (80.1%) ions was observed by NPBC at doses of 40 g L^{-1}. It suggests that the active spots of adsorbent's surfaces are insufficient to adsorb all of the metal ions in the solution at low dosages. The removal efficiency intensely rises with increasing adsorbent due to the presence of more unoccupied active sites on the surface of NPBC and SABC [59]. Beyond 10 g L^{-1} and 20 g L^{-1} for SABC removal percent of Pb(II) and Cd(II) was correspondingly attained worthy value (> 80%) representing the saturation of the active sites [16, 45]. Additionally, there is a drop in the metal ion adsorption capacity as the adsorbent dosage increases (Fig. S2i, j). This could be because a larger adsorbent dose results in more vigorous sites for adsorption, which lowers the adsorption capacity per unit mass. The adsorbed metal ions on the surface of the adsorbent and the remaining heavy metal ions in bulk solutions continue to be in balance.

3.3 Kinetics and isotherm models

Fig. S3 (supplementary information) depicts the effects of different reaction times (0 to 360 min) on adsorption of Pb(II) and Cd(II) by NPBC and SABC. The calculation of adsorption kinetic models (PFO, PSO, Elovich kinetic, and

Table 2 Kinetic model and isotherm parameters for Pb(II) and Cd(II) adsorption onto the nitrogen-purged biochar (NPBC) and steam-activated biochar (SABC)

Model	Parameter	Heavy metals			
		Pb(II)		Cd(II)	
		NPBC	SABC	NPBC	SABC
Pseudo-first order kinetic model	q_e(mg g^{-1})	4.814	4.833	0.202	0.236
	k_1 (min^{-1})	0.093	0.101	0.056	0.057
	χ^2	4.99E-03	2.67E-03	6.02E-05	2.85E-05
	Adj. R^2	0.998	0.999	0.989	0.996
Pseudo-second order kinetic model	q_e(mg g^{-1})	4.989	4.983	0.215	0.251
	k_2 (g mg^{-1} min^{-1})	0.042	0.051	0.445	0.382
	χ^2	1.23E-02	1.40E-02	2.44E-04	1.84E-04
	R^2	0.996	0.995	0.954	0.974
Elovich kinetic model	α (mg g^{-1} min^{-1})	6865.83	86,582.96	0.572	0.602
	β (g mg^{-1})	3.151	3.697	42.042	35.41
	χ^2	5.66E-02	5.26E-02	5.40E-04	4.95E-04
	R^2	0.980	0.982	0.898	0.930
Langmuir isotherm	q_{max} (mg g^{-1})	452.13	1117.00	314.91	470.43
	K_l (L mg^{-1})	0.003	7.76E-05	2.10E-05	1.60E-04
	χ^2	0.14	0.453	2.21E-04	2.41E-04
	R^2	0.996	0.989	0.996	0.997
Freundlich isotherm	K_f (mg g^{-1}) $(mg^{-1})^{1/n}$	0.202	0.094	0.061	0.067
	n	1.219	1.019	0.965	0.949
	$\chi 2$	0.37	0.539	2.29E-04	1.83E-04
	R^2	0.990	0.987	0.996	0.997
Redlich–Peterson isotherm	K_{rp} (L g^{-1})	0.094	14.38	0.208	0.286
	α $(L\ mg^{-1})^{\beta}$	7.59E-12	151.80	2.150	2.795
	β	4.583	0.019	1.08E-17	7.08E-16
	χ^2	0.016	0.539	2.66E-04	2.87E-04
	R^2	1.000	0.987	0.995	0.996

intra-particle diffusion model) is presented in Table S2 (supplementary information). Among the four kinetic models, PFO, PSO, and Elovich kinetic models were well fitted (higher R^2 and low χ^2 value) to Pb(II) and Cd(II) adsorption on NPBC and SABC (Table 2). The PFO kinetic model was best fitted (R^2 0.99; low χ^2 value), which indicated the predominance of HM physisorption on both NPBC and SABC which is the rate limiting mechanism involving intermolecular van der Waals forces [60]. With increased adsorbate-adsorbent contact time, the kinetic trend of Cd(II) and Pb(II) adsorption on SABC and NPBC dropped and reached a plateau (Fig. S3). This may be due to proportionally decreased adsorption amount with decreased the ability of both the adsorbents to adsorb, which was consistent with earlier research [61, 62]. The amount of Cd(II) and Pb(II) adsorption increased by prolonging the reaction time (Fig. S3). Electrons are transferred, exchanged, and co-occurring throughout the adsorption procedure [25, 29]. A number of variables, such as the size of the hydrated ions, hydration energy, electronegativity, and the metal ions activity, contributed to the greater amount of Pb(II) adsorption in comparison with Cd(II) [63]. Additionally, due to Pb(II)'s mobility in the aqueous solution, its activity is also increased [64].

Using different initial concentrations of Pb(II) and Cd(II) from 5 to 200 mg L^{-1} and 1 to 10 mg L^{-1}, respectively, the Langmuir, Freundlich, Redlich–Peterson, and Temkin adsorption isotherm equation models were utilized to determine the interaction between the metals and the adsorbent (NPBC and SABC) (Table S3, supplementary information). The adsorptions of Pb(II) and Cd(II) molecules over a surface of the adsorbents have uniform energy sites that are equally available for interaction according to the Langmuir model [65]. Adsorption occurred in a multiple-layer on an irregular surface in the case of the Freundlich isotherm [65]. Graphs of HM adsorbed (q_t) versus equilibrium HM concentration (C_e) were plotted to show the adsorption isotherm model and demonstrated in Fig. S4 (supplementary information). The intercept of the linear plots is used to compute the values of q_{max}, which indicated a maximum adsorption of the adsorbents. SABC had 1.5 and 0.5 times higher q_{max} values for Pb(II) and Cd(II) (1117 and 470.43 mg g^{-1}, respectively) as compared to the NPBC (452.13 and 314.91 mg g^{-1}, respectively). The R^2 values of SABC obtained for the Pb(II) and Cd(II) were 0.989 and 0.997, whereas R^2 values for NPBC for both Pb(II) and Cd(II) were 0.996 for the Langmuir isotherm (Table 2). Thus, the utmost fit isotherm for removal of Pb(II) by NPBC and SABC was Redlich-Peterson and Langmuir models, respectively. In the Freundlich isotherm model, the values of n are equal to or more than 1, indicating favourability of linear adsorption on heterogeneous surfaces [66]. While, R^2 values are the same in Langmuir as well as Freundlich isotherm models for Cd(II) adsorption by NPBC and SABC. So, the best fit isotherm model for the removal of Cd(II) by NPBC and SABC were both Freundlich and Langmuir models. Therefore, the adsorption mechanism for Cd(II) and Pb(II) by BCs showed a merger of physical adsorption and chemisorption [67]. Moreover, lower R^2 values indicated Pb(II) and Cd(II) adsorption did not follow the Temkin isotherm model. Table 3 lists previous studies conducted by different researchers on the removal of Pb(II) and Cd(II) using alternative and affordable adsorbents.

Table 3 Comparing maximum adsorption capacity (q_{max}) of adsorbents of present work with other literatures for Pb(II) and Cd(II) removal

Adsorbents	Contact Time (minutes)	pH	q_{max} (mg g^{-1})		References
			Pb(II)	Cd(II)	
Acid activated wheat straw biochar	90	6.0	-	74.6	[16]
H_3PO_4-modified chicken feather biochar	120	5.0	55.4	7.84	[74]
Activated carbon prepared from *Eucalyptus sp.*	120	8.0	9.26	6.17	[75]
Thiol-modified rice straw biochar	120	5.0	61.4	45.1	[76]
NaOH modified coffee husk biochar	60	7.0	139.5	116.3	[18]
Surface modified magnetic biochar	120	5.5	61.3	53.8	[77]
Poplar saw dust biochar	600	5.0	62.7	49.3	[78]
15%Mg modified corncob biochar	360	6.0	526.2	179.0	[79]
Mg-coated coconut shell biochar	840	5.0	532.3	205.1	[80]
Banana stem-leaf biochar	200	4.0 for Pb(II) 8.0 for Cd(II)	302.2	32.0	[60]
Amino-modified cornstalk biochar	180	7.0	-	375.6	[46]
Mn-modified rice straw biochar	360	5.0	214.4	165.7	[70]
Nitrogen-purged wheat straw biochar (NPBC)	60	5.0	452.1	314.9	Present study
Steam activated wheat straw biochar (SABC)	60	5.0	1117.0	470.4	Present study

Table 4 Estimated thermodynamic parameters for Pb(II) and Cd(II) adsorption onto the nitrogen-purged biochar (NPBC) and steam-activated biochar (SABC)

Adsorbents	Thermodynamic parameters	Heavy metals					
		Pb(II)			Cd(II)		
	Temperature (K)	298	308	318	298	308	318
NPBC	ΔG (KJ mol^{-1})	− 8.76	− 7.84	− 7.66	− 1.72	− 0.79	− 0.38
	ΔH (KJ mol^{-1})	− 25.12			− 21.54		
	ΔS (J mol^{-1} K^{-1})	55.3			66.8		
	R^2	0.87			0.95		
SABC	ΔG (KJ mol^{-1})	− 8.62	− 8.35	-7.35	− 2.530	− 1.81	− 0.92
	ΔH (KJ mol^{-1})	− 25.12			− 26.46		
	ΔS (J mol^{-1} K^{-1})	55.30			80.20		
	R^2	0.870			0.990		

3.4 Thermodynamics of Pb(II) and Cd(II) adsorption

The nature and dimensions of thermodynamic parameters show a mechanism pertaining to the creation of an adsorbed layer and demonstrate the viability of the adsorption process [61]. Table 4 presents the findings for the thermal properties acquired for NPBC and SABC. The ΔG values of both adsorbents were negative, indicating that the adsorption process of Pb(II) and Cd(II) is both spontaneous and thermodynamically promising. The ΔG value enhanced with an increase in temperature from 298 to 318 K, which indicated that the adsorption is more favourable at lower temperatures [68]. Moreover, adsorbate may desorb from the adsorbent's surface at higher T due to the kinetic energy of the adsorbate suppressing the forces of adsorption [69]. In other words, a higher driving force for adsorption is indicated by a higher negative ΔG value, which leads to an increased adsorption capacity. Pb(II) adsorption on both the adsorbents is comparatively more favourable than the Cd(II). The ΔS values showed the modification in entropy throughout an adsorption process and those were 55.3 and 66.8 J mol^{-1} K^{-1} for adsorption of Pb(II) and Cd(II) on NPBC, whereas ΔS values were 63.60 and 80.20 J mol^{-1} K^{-1} for adsorption of Pb(II) and Cd(II) on SABC. The positive ΔS values represent the adsorbent's affinity for the adsorbate and the increase in ΔS values indicated randomness of ions with raised T and resulted in decreased adsorption of ions. The solid–liquid interface exhibits structural alterations, as suggested by the positive ΔS values found for both the materials [55]. The negative values of ΔH illustrated exothermic adsorption of Cd(II) and Pb(II) ions on NPBC and SABC (Table 4). An exothermic reaction implicates a reduction in surface energy, which appears as heat and occurs during adsorption with non-ionic exchange [70]. The adsorption is preferred at lower T through the physisorption method [71]. When the change in ΔH is less than 21 kJ mol^{-1}, it means that during the adsorption process, physical adsorption

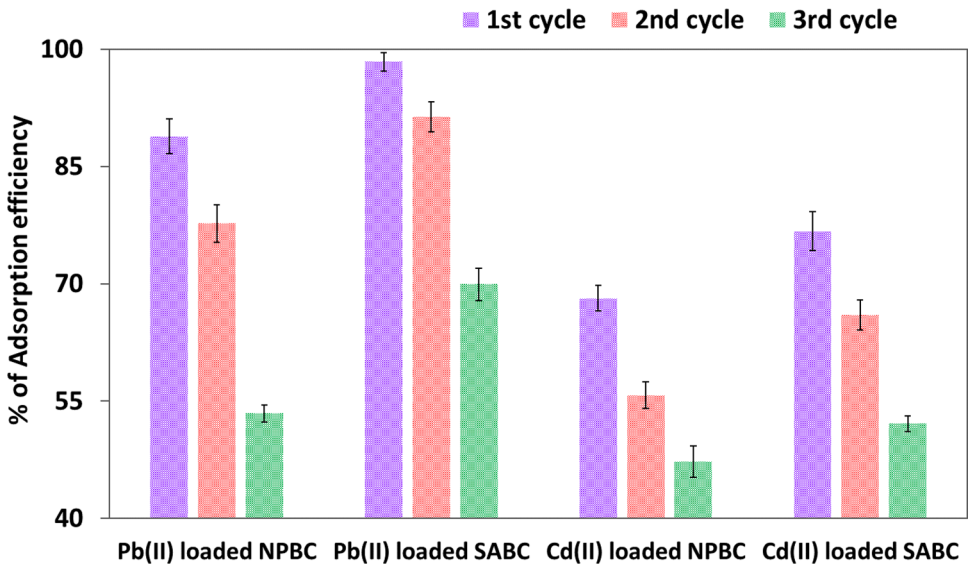

Fig. 5 Pb(II) and Cd(II) adsorption capacities of NPBC and SABC after three consecutive adsorption–desorption cycles. Vertical error bars denote standard deviation which represents the variation relative to corresponding mean point where n = 3

is more resilient than chemisorption. There is still much to learn about the phenomena underlying these processes. Nevertheless, the literature claims that exothermic processes allow metallic ions to get onto the adsorbent's surface and adsorb ions in the liquid phase.

3.5 Desorption and reusability performances

After three adsorption–desorption intervals, the adsorption efficiency of both NPBC and SABC was lower than their initial maximum adsorption efficiency, according to their reusability results (Fig. 5). There were fewer active adsorption sites readily accessible on the surface of the adsorbent due to decreased removal of bound metal ions throughout the desorption process [72]. In the first cycle, the adsorption efficiency by SABC was approximately 98.3% for Pb(II) and 76.7% for Cd(II). After three subsequent adsorption–desorption cycles, SABC retained adsorption efficiency up to 70.1 and 52.3% for Pb(II) and Cd(II), respectively. Similarly, a substantial change of Pb(II) (88.8 to 53.4%) and Cd(II) (68.1 to 47.2%) in the adsorption ability of NPBC was observed after three sequential adsorption–desorption periods, which demonstrates that, in comparison to NPBC, SABC have much more possibility of renewal and later use as adsorbent materials. The reusability of these adsorbents for Pb(II) and Cd(II), are sustainable as the adsorbent is recycled efficiently and there is no chances of producing any kind of post-regenerative chemicals. Moreover, wheat straw biochar is made from agricultural biomass which is sustainable in nature. Although, adsorption–desorption investigations using larger concentrations of desorbing agents may lead to efficient adsorbent renewal and more effective metal recovery.

3.6 Mechanism of Pb(II) and Cd(II) adsorption for NPBC and SABC

Overall, Pb(II) and Cd(II) adsorption mechanisms on NPBC and SABC may include physical adsorption in the structural pores of the biochars, as well as chemical adsorption mechanisms like electrostatic attraction, co-precipitation, complexation, ion exchange, etc. (Fig. 6). Van der Waals force and specific surface area are the main factors in physical adsorption, and it requires the emergence of chemical bonds with the diffusion of metal ions in the sorbent's pores. In addition, Pb(II) and Cd(II) are extracted from aqueous solutions via concurrent precipitation, ion exchange, complexation, and electrostatic interaction. Electrostatic attraction between the negatively charged biochar and positively charged Pb(II)

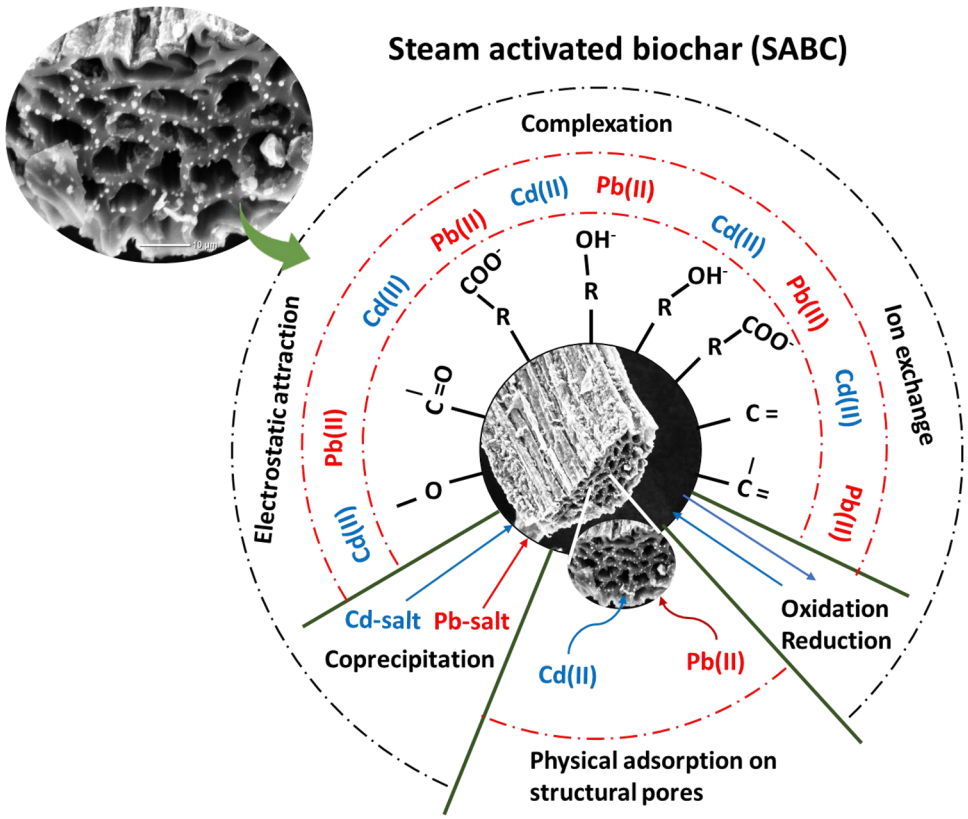

Fig. 6 Proposed mechanism of Pb(II) and Cd(II) adsorption on SABC

and Cd(II) ions limits the mobilization of these potentially toxic HM [73]. As pH rises, the N-containing functional groups in NPBC, viz., pyridinic-N and amino group gradually deprotonate, improving the material's ability to adsorb Pb(II) and Cd(II) ions. The oxygen-containing functional groups in the SABC, such as -COOH, R-COO-R, -CHO, and C_6H_5OH, allow it to bind with Pb(II) and Cd(II). This oxygen content may cause the BC's surface to be more oxidized, which would improve the metal complexation. Additionally, precipitation is one of the major mechanisms that forms mineral precipitates into the solution or on the surface of both BC. In general, industrial contamination is the main source of Pb(II) and Cd(II) contamination in the natural municipal wastewater. Buzier et al. [81], Gourlay-Francé et al. [82] Hargreaves et al. [83] has reported that adsorption and coagulation is the best mechanism to remove Pb and Cd from the natural wastewaters.

4 Conclusions

Pb(II) and Cd(II) adsorption behaviors on novel biochars synthesized under two distinct activator moduli were the focus of this investigation. Results from XRD, SEM, and EGME showed that SABC had higher specific surface area, more porous and amorphous structure than NPBC. The batch adsorption studies found that the ideal pH was 8, the temperature was 298 K, and the NPBC and SABC doses were 20 g L^{-1} and 10 g L^{-1} for Pb(II), respectively. For Cd(II), the corresponding NPBC and SABC doses were 30 g L^{-1} and 20 g L^{-1}. For Pb(II) and Cd(II), SABC demonstrated a greater adsorption capacity of 1117 and 470 mg g^{-1}, respectively, than NPBC, which had an adsorption capacity of 452 and 314 mg g^{-1}. In addition, compared to NPBC, SABC exhibits superior repurposing and further use potential (3 times reusability) as adsorbent materials. This study explores the use of biochars as a non-toxic, scalable, and effective adsorbent for removing Pb(II) and Cd(II) from wastewater.

Acknowledgements The authors would like to acknowledge technical and management support from ICAR-Indian Institute of Soil Science, Bhopal for providing internal facilities for this research work. The authors would also sincerely acknowledge CSIR-Advanced Materials and Process Research Institute (AMPRI), Bhopal, India for providing instrument facilities.

Author contribution Madhumonti Saha: Conceptualization, Investigation, Editing, and Writing—original draft; Pabitra Kumar Biswas: Supervision and Reviewing; Jayanta Kumar Saha: Supervision and Data curation; Abhijit Sarkar: Formal analysis, Validation, Reviewing and Editing; Sandip Mandal: Biochar preparation, Resources and Reviewing; Dinesh Kumar Yadav: Resources and Editing; Sangeeta Lenka: Reviewing and Characterization techniques; M Vassanda Coumar: Resources and Editing; Biraj Bandhu Basak: Reviewing and Editing.

Data availability Data is provided within the manuscript or supplementary information files.

Declarations

Competing interests The authors declare no competing interests.

References

1. Pratap B, Kumar S, Nand S, Azad I, Bharagava RN, Ferreira LFR, Dutta V. Wastewater generation and treatment by various eco-friendly technologies: possible health hazards and further reuse for environmental safety. Chemo. 2023;313:137547. https://doi.org/10.1016/j.chemosphere.2022.137547.
2. Minhas PS, Saha JK, Dotaniya ML, Sarkar A, Saha M. Wastewater irrigation in India: current status, impacts and response options. Sci Total Environ. 2022;808:152001. https://doi.org/10.1016/j.scitotenv.2021.152001.
3. Hussain MI, Muscolo A, Farooq M, Ahmad W. Sustainable use and management of non-conventional water resources for rehabilitation of marginal lands in arid and semiarid environments. Agril Water Manag. 2019;221:462–76. https://doi.org/10.1016/j.agwat.2019.04.014.
4. Huang JL, Li ZY, Mao JY, Chen ZM, Liu HL, Liang GY, Zhang DB, Wen PJ, Mo ZY, Jiang YM. Contamination and health risks brought by arsenic, lead and cadmium in a water-soil-plant system nearby a non-ferrous metal mining area. Ecotoxicol Environ Saf. 2024;270:115873. https://doi.org/10.1016/j.ecoenv.2023.115873.

5. USEPA. National recommended water quality criteria. EPA–822-R-02–047. Office of Water, Office of Science and Technology; 2002.
6. Kafouris D, Christoforou E, Stefani D, Sarandi A, Stavroulakis G, Christou E, Yiannopoulos S. Lead, cadmium and mercury determination and human health risk assessment in foods from Cyprus. J Food Compos Anal. 2024;128:106007. https://doi.org/10.1016/j.jfca.2024.106007.
7. Shrestha R, Ban S, Devkota S, Sharma S, Joshi R, Tiwari AP, Joshi MK. Technological trends in heavy metals removal from industrial wastewater: a review. J Environ Chem Engg. 2021;9:105688. https://doi.org/10.1016/j.jece.2021.105688.
8. Juve JMA, Christensen FMS, Wang Y, Wei Z. Electrodialysis for metal removal and recovery: a review. Chem Engg J. 2022;435:134857. https://doi.org/10.1016/j.cej.2022.134857.
9. Kim JG, Ku J, Jung J, Park YS, Choi GH, Hwang SS, Lee JH, Lee AS. Ion-exchangeable and sorptive reinforced membranes for efficient electrochemical removal of heavy metal ions in wastewater. J Clean Prod. 2024;438:140779. https://doi.org/10.1016/j.jclepro.2024.140779.
10. Singh A, Shah SS, Sharma C, Gupta V, Sundramoorthy AK, Kumar P, Arya S. An approach towards different techniques for detection of heavy metal ions and their removal from waste water. J Environ Chem Eng. 2024. https://doi.org/10.1016/j.jece.2024.113032.
11. Chai WS, Cheun JY, Kumar PS, Mubashir M, Majeed Z, Banat F, Ho SH, Show PL. A review on conventional and novel materials towards heavy metal adsorption in wastewater treatment application. J Clean Prod. 2021;296:126589. https://doi.org/10.1016/j.jclepro.2021.126589.
12. Jiang J, Shi Y, Ma NL, Ye H, Verma M, Ng HS, Ge S. Utilizing adsorption of wood and its derivatives as an emerging strategy for the treatment of heavy metal-contaminated wastewater. Environ Pollut. 2024;340:122830. https://doi.org/10.1016/j.envpol.2023.122830.
13. Karić N, Maia AS, Teodorović A, Atanasova N, Langergraber G, Crini G, Ribeiro AR, Đolić M. Bio-waste valorisation: agricultural wastes as biosorbents for removal of (in) organic pollutants in wastewater treatment. Chem Eng J Adv. 2022;9:100239. https://doi.org/10.1016/j.ceja.2021.100239.
14. Hamid Y, Chen Y, Lin Q, Haris M, Usman M, Rashid MS, Anastopoulos I, Hussain B, Ali HM, Hannan F, Yin X. Functionality of wheat straw-derived biochar enhanced its efficiency for actively capping Cd and Pb in contaminated water and soil matrices: Insights through batch adsorption and flow-through experiments. Chemosphere. 2024. https://doi.org/10.1016/j.chemosphere.2024.142770.
15. Nassef HM, Al-Hazmi GA, Alayyafi AA, El-Desouky MG, El-Bindary AA. Synthesis and characterization of new composite sponge combining of metal-organic framework and chitosan for the elimination of Pb (II), Cu (II) and Cd (II) ions from aqueous solutions: batch adsorption and optimization using Box-Behnken design. J Mol Liq. 2024;394:123741. https://doi.org/10.1016/j.molliq.2023.123741.
16. Naeem MA, Imran M, Amjad M, Abbas G, Tahir M, Murtaza B, Zakir A, Shahid M, Bulgariu L, Ahmad I. Batch and column scale removal of cadmium from water using raw and acid activated wheat straw biochar. Water. 2019;11(7):1438. https://doi.org/10.3390/w11071438.
17. Ahmed MJ, Anastopoulos I, Kalderis D, Haris M, Usman M. Insight into the wheat residues-derived adsorbents for the remediation of organic and inorganic aquatic contaminants: a review. Environ Res. 2024. https://doi.org/10.1016/j.envres.2024.118507.
18. Thi Quyen V, Pham TH, Kim J, Thanh DM, Thang PQ, Van Le Q, Jung SH, Kim T. Biosorbent derived from coffee husk for efficient removal of toxic heavy metals from wastewater. Chemosphere. 2021;284:131312. https://doi.org/10.1016/j.chemosphere.2021.131312.
19. Shahrokhi-Shahraki R, Benally C, El-Din MG, Park J. High-efficiency removal of heavy metals using tire-derived activated carbon vs commercial activated carbon: insights into the adsorption mechanisms. Chemosphere. 2020;264:128455. https://doi.org/10.1016/j.chemosphere.2020.128455.
20. Ding C, Gan Y, Luo J, Cui Y. Wheat straw biochar and its performance in treatment of phenanthrene containing water and microbial remediation of phenanthrene contaminated soil. Fron Environ Sci. 2022;10:1039603. https://doi.org/10.3389/fenvs.2022.1039603.
21. Shi W, Wang H, Yan J, Shan L, Quan G, Pan X, Cui L. Wheat straw derived biochar with hierarchically porous structure for bisphenol A removal: preparation, characterization, and adsorption properties. Separ Purif Technol. 2022;289:120796. https://doi.org/10.1016/j.seppur.2022.120796.
22. Riseh RS, Vazvani MG, Hassanisaadi M, Thakur VK. Agricultural wastes: a practical and potential source for the isolation and preparation of cellulose and application in agriculture and different industries. Ind Crops Prod. 2024;208:117904. https://doi.org/10.1016/j.indcrop.2023.117904.
23. Dutta A, Patra A, Hazra KK, Nath CP, Kumar N, Rakshit A. A state-of-the-art review in crop residue burning in India: previous knowledge, present circumstances and future strategies. Environ Chall. 2022;8:100581. https://doi.org/10.1016/j.envc.2022.100581.
24. Lopes AA, Tasneem D, Viriyavipart A. Determinants of wheat residue burning: evidence from India. PLoS ONE. 2023;18(12): e0296059. https://doi.org/10.1371/journal.pone.0296059.
25. Basak BB, Sarkar B, Saha A, Sarkar A, Mandal S, Biswas JK, Wang H, Bolan NS. Revamping highly weathered soils in the tropics with biochar application: what we know and what is needed. Sci Tot Environ. 2022;822:153461. https://doi.org/10.1016/j.scitotenv.2022.153461.
26. Biswal BK, Balasubramanian R. Use of biochar as a low-cost adsorbent for removal of heavy metals from water and wastewater: a review. J Environ Chem Eng. 2023. https://doi.org/10.1016/j.jece.2023.110986.
27. Zhao J, Shen XJ, Domene X, Alcañiz JM, Liao X, Palet C. Comparison of biochars derived from different types of feedstock and their potential for heavy metal removal in multiple-metal solutions. Sci Rep. 2019;9(1):9869. https://doi.org/10.1038/s41598-019-46234-4.
28. Ghanmi I, Sassi W, Oulego P, Collado S, Ghorbal A, Díaz M. A comparative study of batch adsorption process of biomass and its biochar during indigo carmine removal. Biomass Conv Bioref. 2023;1:1–3. https://doi.org/10.1007/s13399-023-05045-4.
29. Amen R, Yaseen M, Mukhtar A, Klemeš JJ, Saqib S, Ullah S, Al-Sehemi AG, Rafiq S, Babar M, Fatt CL, Ibrahim M, Asif S, Qureshi KS, Akbar MM, Bokhari A. Lead and cadmium removal from wastewater using eco-friendly biochar adsorbent derived from rice husk, wheat straw, and corn cob. Clean Eng Technol. 2020;1:100006. https://doi.org/10.1016/j.clet.2020.100006.
30. Colomba A, Berruti F, Briens C. Model for the physical activation of biochar to activated carbon. J Anal Appl Pyroly. 2022;168:105769. https://doi.org/10.1016/j.jaap.2022.105769.
31. Bardha A, Prasher S, Villarta J, Francis MS, Khirpin CY, Mehlem JJ, Dumont MJ. Nut shell and grain husk waste biochar as carbon black replacements in styrene-butadiene rubber composites and improvements through steam activation. Ind Crops Prod. 2023;203:117180. https://doi.org/10.1016/j.indcrop.2023.117180.
32. Mandal S, Bhattacharya TK, Verma AK, Haydary J. Optimization of process parameters for bio-oil synthesis from pine needles (Pinus roxburghii) using response surface methodology. Chem Pap. 2018;72:603–16. https://doi.org/10.1007/s11696-017-0306-5.
33. ICAR-CIAE, annual report, 2020. https://ciae.icar.gov.in/prominent_tech_aep.html. Accessed 2 Mar 2024.

34. Carter DL, Mortland MM, Kemper WD. Specific surface. In: Methods of soil analysis", Chapter 16, agronomy No. 9, Part 1. 2nd ed. Madison: American Society of Agronomy; 1986.
35. Gorgievski M, Božić D, Stanković V, Štrbac N, Šerbula S. Kinetics equilibrium and mechanism of Cu^{2+}, Ni^{2+} and Zn^{2+} ions biosorption using wheat straw. Eco Engg. 2013;58:113–21. https://doi.org/10.1016/j.ecoleng.2013.06.025.
36. Sriram G, Bhat MP, Kigga M, Uthappa UT, Jung HY, Kumeria T, Kurkuri MD. Amine activated diatom xerogel hybrid material for efficient removal of hazardous dye. Mater Chem Phys. 2019;235:121738. https://doi.org/10.1016/j.matchemphys.2019.121738.
37. Wang J, Guo X. Adsorption kinetic models: physical meanings, applications, and solving methods. J Hazard Mater. 2020;390:122156. https://doi.org/10.1016/j.jhazmat.2020.122156.
38. Wang J, Guo X. Adsorption isotherm models: classification, physical meaning, application and solving method. Chemosphere. 2020;258:127279. https://doi.org/10.1016/j.chemosphere.2020.127279.
39. Kavci E. Malachite green adsorption onto modified pine cone: isotherms, kinetics and thermodynamics mechanism. Chem Engg Commun. 2020;208(3):318–27. https://doi.org/10.1080/00986445.2020.1715961.
40. Chen D, Cen K, Zhuang X, Gan Z, Zhou J, Zhang Y, Zhang H. Insight into biomass pyrolysis mechanism based on cellulose, hemicellulose, and lignin: evolution of volatiles and kinetics, elucidation of reaction pathways, and characterization of gas, biochar and bio-oil. Combust Flame. 2022;242:112142. https://doi.org/10.1016/j.combustflame.2022.112142.
41. Khan HA, Naqvi SR, Mehran MT, Khoja AH, Niazi MBK, Juchelková D, Atabani A. A performance evaluation study of nano-biochar as a potential slow-release nano-fertilizer from wheat straw residue for sustainable agriculture. Chemosphere. 2021;285:131382. https://doi.org/10.1016/j.chemosphere.2021.131382.
42. Li H, Dong X, da Silva EB, de Oliveira LM, Chen Y, Ma LQ. Mechanisms of metal sorption by biochars: biochar characteristics and modifications. Chemosphere. 2017;178:466–78. https://doi.org/10.1016/j.chemosphere.2017.03.072.
43. Das DS, Venkata TB. Specific surface area of plastic clays from equilibrium sediment volume under salt environment. Geotech Testing J. 2021;44(5):1484–500. https://doi.org/10.1520/GTJ20200190.
44. Lou K, Rajapaksha AU, Ok YS, Chang SX. Pyrolysis temperature and steam activation effects on sorption of phosphate on pine sawdust biochars in aqueous solutions. Chem Spec Bioavail. 2016;28(1–4):42–50. https://doi.org/10.1080/09542299.2016.1165080.
45. Janu R, Mrlik V, Ribitsch D, Hofman J, Sedláček P, Bielská L, Soja G. Biochar surface functional groups as affected by biomass feedstock, biochar composition and pyrolysis temperature. Carbon Res Conver. 2021;4:36–46. https://doi.org/10.1016/j.crcon.2021.01.003.
46. Ma F, Zhao H, Zheng X, Zhao B, Diao J, Jiang Y. Enhanced adsorption of cadmium from aqueous solution by amino modification biochar and its adsorption mechanism insight. J Environ Chem Eng. 2023;11(3):109747. https://doi.org/10.1016/j.jece.2023.109747.
47. Kumar A, Bhattacharya T. Removal of arsenic by wheat straw biochar from soil. Bull Environ Contam Toxicol. 2022;108(3):415–22. https://doi.org/10.1007/s00128-020-03095-2.
48. Rathnayake D, Rego F, Van Poucke R, Bridgwater AV, Mašek O, Meers E, Wang J, Yang Y, Ronsse F. Chemical stabilization of Cd-contaminated soil using fresh and aged wheat straw biochar. Environ Sci Pollut Res. 2021;28:10155–66. https://doi.org/10.1007/s11356-020-11574-6.
49. Vaghela DR, Pawar A, Sharma D. Effectiveness of wheat straw biochar in aqueous Zn removal: correlation with biochar characteristics and optimization of process parameters. Bio Energy Res. 2023;16(1):457–71. https://doi.org/10.1007/s12155-022-10471-9.
50. Burachevskaya M, Minkina T, Bauer T, Lobzenko I, Fedorenko A, Mazarji M, Sushkova S, Mandzhieva S, Nazarenko A, Butova V, Wong MH. Fabrication of biochar derived from different types of feedstocks as an efficient adsorbent for soil heavy metal removal. Sci Rep. 2023;13(1):2020. https://doi.org/10.1038/s41598-023-27638-9.
51. Sireesha S, Upadhyay U, Sreedhar I. Comparative studies of heavy metal removal from aqueous solution using novel biomass and biochar-based adsorbents: characterization, process optimization, and regeneration. Biomass Convers Biorefin. 2022. https://doi.org/10.1007/s13399-021-02186-2.
52. Liao W, Zhang X, Ke S, Shao J, Yang H, Zhang S, Chen H. Effect of different biomass species and pyrolysis temperatures on heavy metal adsorption, stability and economy of biochar. Ind Crops Prod. 2022;186:115238. https://doi.org/10.1016/j.indcrop.2022.115238.
53. Naseem K, Begum R, Wu W, Usman M, Farooqi JH. Adsorptive removal of heavy metal ions using polystyrene-poly (N-isopropylmethacrylamide-acrylic acid) core/shell gel particles: adsorption isotherms and kinetic study. J Mol Liq. 2019;277:522–31. https://doi.org/10.1016/j.molliq.2018.12.054.
54. El Maghrabi AH, Marzouk MA, Elbably MA, Hassouna MEM. Biosorption of manganese by amended Aspergillus versicolor from polluted water sources. Nat Environ Pollut Technol. 2020;9(4):1645–56. https://doi.org/10.46488/NEPT.2020.v19i04.000.
55. Panda L, Jena SK, Rath SS, Misra PK. Heavy metal removal from water by adsorption using a low-cost geopolymer. Environ Sci Pollut Res. 2020;27:24284–98. https://doi.org/10.1007/s11356-020-08482-0.
56. Teng D, Zhang B, Xu G, Wang B, Mao K, Wang J, Sun J, Feng X, Yang Z, Zhang H. Efficient removal of Cd(II) from aqueous solution by pinecone biochar: sorption performance and governing mechanisms. Environ Pollut. 2020;265:115001. https://doi.org/10.1016/j.envpol.2020.115001.
57. Wei S, Du G, Li C, Zhang L, Li J, Mao A, He C. Removal mechanism of Pb (ii) from soil by biochar-supported nanoscale zero-valent iron composite materials. RSC Adv. 2024;14(26):18148–60. https://doi.org/10.1039/D4RA03357D.
58. Sen TK. Agricultural solid wastes based adsorbent materials in the remediation of heavy metal ions from water and wastewater by adsorption: a review. Mol. 2023;28(14):5575. https://doi.org/10.3390/molecules28145575.
59. Fatma UK, Nizami G, Ahamad S, Saquib M, Hussain MK. Activated Green Tamarind Pulp (AGTP) as an efficient adsorbent for removal of Pb2+, Cu2+, Zn2+ & Ni2+ from contaminated water. J Water Process Engg. 2024;59:105048. https://doi.org/10.1016/j.jwpe.2024.105048.
60. Liu X, Li G, Chen C, Zhang X, Zhou K, Long X. Banana stem and leaf biochar as an effective adsorbent for cadmium and lead in aqueous solution. Sci Rep. 2022;12(1):1584. https://doi.org/10.1038/s41598-022-05652-7.
61. Mukhopadhyay R, Adhikari T, Sarkar B, Barman A, Paul R, Patra AK, Sharma PC, Kumar P. Fe-exchanged nano-bentonite outperforms Fe_3O_4 nanoparticles in removing nitrate and bicarbonate from wastewater. J Hazard Mater. 2019;376:141–52. https://doi.org/10.1016/j.jhazmat.2019.05.025.
62. Kwikima MM, Chebude Y, Meshesha BT. Kinetics, adsorption isotherms, thermodynamics, and desorption studies of cadmium removal from aqueous solutions using bamboo sawdust/rice husk biochar. Biomass Convers Biorefin. 2023;13(11):9367–79. https://doi.org/10.1007/s13399-022-03472-3.

63. He F, Ma B, Wang C, Chen Y, Hu X. Adsorption of Pb (II) and Cd (II) hydrates via inexpensive limonitic laterite: adsorption characteristics and mechanisms. Sep Purif Technol. 2023;310:123234. https://doi.org/10.1016/j.seppur.2023.123234.
64. Das L, Saha N, Ganguli A, Das P, Bhowal A, Bhattacharjee C. Calcium alginate–bentonite/activated biochar composite beads for removal of dye and Biodegradation of dye-loaded composite after use: synthesis, removal, mathematical modeling and biodegradation kinetics. Environ Tech Innov. 2021;24:101955. https://doi.org/10.1016/j.eti.2021.101955.
65. Manippady SR, Singh A, Basavaraja BM, Samal AK, Srivastava S, Saxena M. Iron–carbon hybrid magnetic nanosheets for adsorption-removal of organic dyes and 4-nitrophenol from aqueous solution. ACS Appl Nano Mat. 2020;3:1571–82. https://doi.org/10.1021/acsanm.9b02348.
66. Sherugar P, Padaki M, Naik NS, George SD, Murthy DHK. Biomass-derived versatile activated carbon removes both heavy metals and dye molecules from wastewater with near-unity efficiency: mechanism and kinetics. Chemosphere. 2022;287(2):132085. https://doi.org/10.1016/j.chemosphere.2021.132085.
67. Qiu B, Tao X, Wang H, Li W, Ding X, Chu H. Biochar as a low-cost adsorbent for aqueous heavy metal removal: a review. J Analyt App Pyroly. 2021;155:105081. https://doi.org/10.1016/j.jaap.2021.105081.
68. Mussa ZH, Al-Ameer LR, Al-Qaim FF, Deyab IF, Kamyab H, Chelliapan S. A comprehensive review on adsorption of methylene blue dye using leaf waste as a bio-sorbent: isotherm adsorption, kinetics, and thermodynamics studies. Environ Monit Assess. 2023;195(8):940. https://doi.org/10.1007/s10661-023-11432-1.
69. Tahoon MA, Siddeeg SM, Salem Alsaiari N, Mnif W, Ben RF. Effective heavy metals removal from water using nanomaterials: a review. Process. 2020;8(6):645. https://doi.org/10.3390/pr8060645.
70. Zeng G, Si M, Dong C, Liao Q, He F, Johnson VE, Yang Z. Adsorption behavior of lead, cadmium, and arsenic on manganese-modified biochar: competition and promotion. Environ Geochem Health. 2024;46(3):86. https://doi.org/10.1007/s10653-024-01865-z.
71. Shahinpour A, Tanhaei B, Ayati A, Beiki H, Sillanpää M. Binary dyes adsorption onto novel designed magnetic clay-biopolymer hydrogel involves characterization and adsorption performance: Kinetic, equilibrium, thermodynamic, and adsorption mechanism. J Mol Liq. 2022;366:120303. https://doi.org/10.1016/j.molliq.2022.120303.
72. Kavand M, Eslami P, Razeh L. The adsorption of cadmium and lead ions from the synthesis wastewater with the activated carbon: optimization of the single and binary systems. J Water Process Eng. 2020;34:101151. https://doi.org/10.1016/j.jwpe.2020.101151.
73. Iamsaard K, Weng CH, Yen LT, Tzeng JH, Poonpakdee C, Lin YT. Adsorption of metal on pineapple leaf biochar: Key affecting factors, mechanism identification, and regeneration evaluation. Bioresource Technol. 2022;344:126131. https://doi.org/10.1016/j.biortech.2021.126131.
74. Chen H, Li W, Wang J, Xu H, Liu Y, Zhang Z, Li Y, Zhang Y. Adsorption of cadmium and lead ions by phosphoric acid-modified biochar generated from chicken feather: selective adsorption and influence of dissolved organic matter. Biores Technol. 2019;292:121948. https://doi.org/10.1016/j.biortech.2019.121948.
75. Gebretsadik H, Gebrekidan A, Demlie L. Removal of heavy metals from aqueous solutions using Eucalyptus Camaldulensis: an alternate low-cost adsorbent. Cogent Chem. 2020;6(1):1720892. https://doi.org/10.1080/23312009.2020.1720892.
76. Fan J, Cai C, Chi H, Reid BJ, Coulon F, Zhang Y, Hou Y. Remediation of cadmium and lead polluted soil using thiol-modified biochar. J Hazard Mater. 2020;388:122037. https://doi.org/10.1016/j.jhazmat.2020.122037.
77. Zahedifar M, Seyedi N, Shafiei S, Basij M. Surface-modified magnetic biochar: Highly efficient adsorbents for removal of Pb (II) and Cd (II). Mater Chem Phys. 2021;271:124860. https://doi.org/10.1016/j.matchemphys.2021.124860.
78. Cheng S, Liu Y, Xing B, Qin X, Zhang C, Xia H. Lead and cadmium clean removal from wastewater by sustainable biochar derived from poplar saw dust. J Clean Prod. 2021;314:128074. https://doi.org/10.1016/j.jclepro.2021.128074.
79. Deng Y, Li X, Ni F, Liu Q, Yang Y, Wang M, Ao T, Chen W. Synthesis of magnesium modified biochar for removing copper, lead and cadmium in single and binary systems from aqueous solutions: adsorption mechanism. Water. 2021;13(5):599. https://doi.org/10.3390/w13050599.
80. Wu J, Wang T, Wang J, Zhang Y, Pan WP. A novel modified method for the efficient removal of Pb and Cd from wastewater by biochar: enhanced the ion exchange and precipitation capacity. Sci Tot Environ. 2021;754:142150. https://doi.org/10.1016/j.scitotenv.2020.142150.
81. Buzier R, Tusseau-Vuillemin MH, Meriadec CMD, Rousselot O, Mouchel JM. Trace metal speciation and fluxes within a major French wastewater treatment plant: Impact of the successive treatments stages. Chemosphere. 2006;65:2419–26.
82. Gourlay-Francé C, Bressy A, Uher E, Lorgeoux C. Labile, dissolved and particulate PAHs and trace metals in wastewater: passive sampling, occurrence, partitioning in treatment plants. Water Sci Technol. 2011;63:1327–33.
83. Hargreaves AJ, Vale P, Whelan J, Constantino C, Dotro G, Campo P, Cartmell E. Distribution of trace metals (Cu, Pb, Ni, Zn) between particulate, colloidal and truly dissolved fractions in wastewater treatment. Chemosphere. 2017;175:239–46.